JACS
JOURNAL OF THE AMERICAN CHEMICAL SOCIETY
Article
pubs.acs.org/JACS

Theoretical Prediction and Experimental Realization of New Stable Inorganic Materials Using the Inverse Design Approach

Andriy Zakutayev,[†] Xiuwen Zhang,[†,‡] Arpun Nagaraja,[∥] Liping Yu,[§] Stephan Lany,[†] Thomas O. Mason,[∥] David S. Ginley,[†] and Alex Zunger*[,§]

[†]National Renewable Energy Laboratory, Golden, Colorado 80401, United States
[‡]Colorado School of Mines, Golden, Colorado 80401, United States
[§]University of Colorado, Boulder, Colorado 80309, United States
[∥]Northwestern University, Evanston, Illinois 60208, United States

Supporting Information

ABSTRACT: Discovery of new materials is important for all fields of chemistry. Yet, existing compilations of all known ternary inorganic solids still miss many possible combinations. Here, we present an example of accelerated discovery of the missing materials using the inverse design approach, which couples predictive first-principles theoretical calculations with combinatorial and traditional experimental synthesis and characterization. The compounds in focus belong to the equiatomic (1:1:1) ABX family of ternary materials with 18 valence electrons per formula unit. Of the 45 possible V−IX−IV compounds, 29 are missing. Theoretical screening of their thermodynamic stability revealed eight new stable 1:1:1 compounds, including TaCoSn. Experimental synthesis of TaCoSn, the first ternary in the Ta−Co−Sn system, confirmed its predicted zincblende-derived crystal structure. These results demonstrate how discovery of new materials can be accelerated by the combination of high-throughput theoretical and experimental methods. Despite being made of three metallic elements, TaCoSn is predicted and explained to be a semiconductor. The band gap of this material is difficult to measure experimentally, probably due to a high concentration of interstitial cobalt defects.

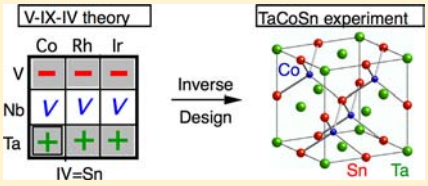

INTRODUCTION

There are vast opportunities for discovery of new compounds in chemistry. For example, many possible inorganic materials that consist of three or more elements are still missing from published resources. Some of these inorganic materials are missing because they have not been synthesized yet, whereas others are missing because they disproportionate into competing phases. The motivation of this work is to show that experimental synthesis of previously missed inorganic compounds can be guided by predictive theoretical first-principles calculations that sort stable versus unstable compounds. This demonstration in the field of inorganic synthetic solid-state chemistry is also important to all other fields of chemistry because of the great potential of abundant and inexpensive computational resources to accelerate the rate of progress.[1,2]

The subject of this paper is ternary equiatomic (1:1:1) ABX materials also known as filled tetrahedral structures,[3,4] Novotny−Juza compounds[5,6] or half-Heusler alloys.[7,8] These materials include families with 8 and 18 valence electrons per formula unit. Each of these families contains many groups, for example, the I−II−V (e.g., LiZnAs) and the I−III−IV (e.g., AgYGe) groups of the 8-electron family, or the V−IX−IV (e.g., NbRhSn) and the IV−IX−V (e.g., TiCoSb) groups of the 18-electron family. Because of the closed-shell s^2p^6 and $s^2p^6d^{10}$ electron count, many 8- and 18-electron ABX materials are semiconductors with thermoelectric,[9] optoelectronic,[10] piezoelectric,[11] ferroelectric,[12] antiferroelectric,[13] topologically insulating,[14,15] and other interesting and useful properties. Other, nonequiatomic compositions of IV−IX−V compounds, such as 2:1:1, 1:2:1, 1:1:2, and so forth, may also exist but are of secondary interest in our present study, as these are expected to have open electronic shell and thus likely to be metals not semiconductors.

A large fraction of the 8- and 18-electron ABX compounds[16] and other novel ternary materials[17] is currently missing from published resources.[18−20] For example, out of 45 possible V−IX−IV 18-electron materials shown in Figure 1, 16 are documented (check-marks on white background), and the remaining 29 are missing ("+" and "−" symbols on gray background). This significant gap in knowledge suggests that the current understanding of chemical trends and crystallographic regularities in such unconventional materials is possibly based on a significantly incomplete body of evidence. This is in sharp contrast to well-established semiconductors with four valence electrons per atom,[21] such as group IV (Si), III−V (GaAs), II−VI (ZnO), I−III−VI_2 ($CuInSe_2$), and I_2−II−IV−VI_4 (Cu_2ZnSnS_4) materials and related ordered defect compounds.[22]

Our understanding of trends and regularities of unconventional materials can be filled by means of the inverse design

Received: November 27, 2012
Published: May 14, 2013

   dx.doi.org/10.1021/ja311599g | J. Am. Chem. Soc. 2013, 135, 10048−10054

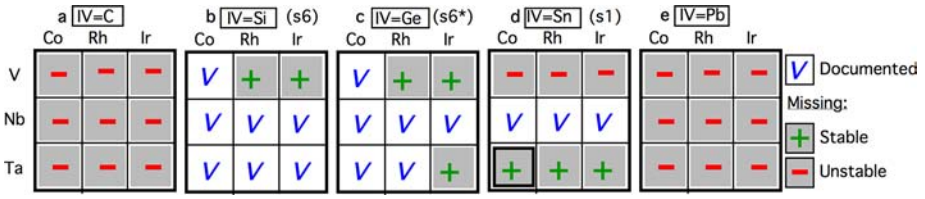

Figure 1. Status of knowledge of 45 equiatomic V−IX−IV materials with V = V, Nb, and Ta, IX = Co, Rh, and Ir, and IV = C (part a), Si (part b), Ge (part c), Sn (part d), and Pb (part e). S1 and S6 refer to the structures of the stable compounds (Figures 2 and 3). The TaCoSn compound marked by a black square has been experimentally synthesized (Figure 4) and predicted to be a semiconductor (Figures 5 and 6).

approach. When applied to the missing materials problem, this approach involves two important steps: (i) theoretical calculations of structure and thermodynamic stability of the missing materials, and (ii) experimental realization of the stable materials in the predicted crystallographic structure. Thus, the inverse design approach reverses the sequence of steps i and ii in traditional materials discovery, where the experimental realization usually precedes the theoretical and computational studies. Recently, the theoretical step (i) of the inverse design approach has been demonstrated by this group[16,17] and other groups.[23,24] However, none of the aforementioned studies contained the experimental step (ii), despite the critical importance of experimental realization of the theoretically predicted materials.[25−27]

This paper demonstrates both theoretical prediction and experimental realization of new stable inorganic materials. The main theoretical result is the prediction of 8 new stable materials out of 29 missing members of the group of 45 equiatomic V−IX−IV compounds (V = V, Nb, and Ta; IX = Co, Rh, and Ir; IV = C, Si, Ge, Sn, and Pb). The main experimental result is the synthesis of TaCoSn, the first ternary material in the Ta−Co−Sn family. We also explain why some of these materials made of three metallic elements are semiconductors and assess optical and alloy properties of these compounds. The significance of this work is that it demonstrates how discovery of new materials and their properties can be accelerated by integration of modern theoretical and experimental methods.

■ THEORETICAL APPROACH

We calculated thermodynamic stability of each missing V−IX−IV compound of 1:1:1 stoichiometry with respect to elemental, binary, and ternary competing phases in two steps. For both steps 1 and 2, we used density functional theory (DFT) corrected for inaccuracies in the elemental-phase reference energies.[28,29] See Theoretical Methods for more information.

In step 1, we calculate the lowest energy crystal structure of each missing material by (1a) comparing its relaxed total energies in a list of previously reported structure types (for example, 41 types for 1:1:1 materials, Table S1, Supporting Information). Subsequently, these results are refined by (1b) a genetic algorithm GSGO search.[30] In this method, one uses DFT combined with genetic algorithm to find with virtually no bias the low energy structure starting from random lattice vectors and random Wyckoff positions. Finally, in step 1c, we examine the dynamic stability of the statically derived minimum energy structure by phonon calculations for the final materials of interest. In this paper, the GSGO search was applied to TaCoSn, and the phonon calculations were done for four compounds in the three-atom AgMgAs-type structure (TaCoSn, TaIrGe, TaRhSn, and TaIrSn, Figure S1, Supporting Information).

In step 2, we compare the energy of the lowest energy crystal structure of each stable compound with the energies of different combinations of competing phases. The energies of all competing phases are calculated as a function of chemical potentials of the involved V, IX, and IV atoms[16] (Figure S2, Supporting Information and Theoretical Methods). In 2a, we consider *known* elemental, binary, and ternary competing phases with structures taken from the Inorganic Crystal Structure Database (ICSD)[18] and other similar resources.[19,20] For example, in the case of TaCoSn, we considered elemental Ta, Co, and Sn and binary CoSn, $CoSn_2$, Co_3Sn_2, $CoSn_3$, Ta_3Sn, $TaSn_2$, Co_3Ta, and Co_2Ta as possible competing phases (in this case, no ternary Ta−Co−Sn compounds had been previously reported). In step 2b, we augment the data set of 2a by unreported competing phases (such as $TaCo_2Sn$ observed in the process of TaCoSn synthesis). The relevant structure types for such previously unreported competing phases are constructed by analogy with reported isovalent compounds and then relaxed to minimize the total energy. For example, we considered $TaCo_2Sn$ (not listed in the ICSD) as a possible competing phase to TaCoSn, in analogy with VCo_2Si, VCo_2Sn, and $NbCo_2Sn$ that are reported in the ICSD.

In the specific case of $TaCo_2Sn$, we calculated the total energy of this material in 66 structure types of the 1:2:1 composition reported in the ICSD (see Table S2, Supporting Information). We found that the lowest energy structure of $TaCo_2Sn$ is the same as that for $NbCo_2Sn$, which supports our approach described above. Further, for the Ta−Co−Sn materials system, we tested our thermodynamic stability calculations approach by a complementary compositionally dependent evolutionary algorithm X-GSGO.[31] Using this algorithm, we are able to vary composition and cell size "on the fly", limitation being the maximal cell size affordable computationally. From the X-GSGO calculations, we found two stable ternary compounds, TaCoSn and $TaCo_2Sn$, and their crystal structures are in agreement with the results from thermodynamic stability calculations described above ($TaCo_2Sn$ was initially synthesized along with TaCoSn and subsequently theoretically considered as a potential competing phase for TaCoSn, as discussed above). From the X-GSGO calculations, we also found that the $TaCo_2Sn$ Heusler compound does not cause disproportionation of the stable TaCoSn half-Heusler material and vice versa, in agreement with the thermodynamic stability analysis results for these two materials (Figure S2, Supporting Information). Overall, these favorable cases of comparison support the validity of our approach to the thermodynamic stability calculations.

■ THEORETICAL RESULTS

Trends in the Thermodynamic Stability. We predicted eight previously missing V−IX−IV compounds with 1:1:1 stoichiometry to be thermodynamically stable, including two

dx.doi.org/10.1021/ja311599g | J. Am. Chem. Soc. 2013, 135, 10048−10054

silicides (VRhSi and VIrSi), three germanides (VRhGe, VIrGe, and TaIrGe), and three stannides (TaCoSn, TaRhSn, and TaIrSn), all indicated by plus signs in Figure 1. These eight new materials represent only a tiny fraction of many stable but missing ABX,[16] A_2BX_4,[17] and other ternary materials that await to be synthesized in laboratories, leaving open many research opportunities in experimental solid-state chemistry. The formation enthalpies and stability areas of all 24 stable equiatomic V−IX−IV materials (16 known and presumed stable plus 8 missing and predicted stable) are listed in Table S3 (Supporting Information). The stability area was defined by the values of chemical potentials of the V, IX, and IV atoms where the V−IX−IV compound is stable (Figure S2, Supporting Information and Theoretical Methods). From the results in Table S3 (Supporting Information), it can be concluded for the V−IX−IV equiatomic ABX materials that (i) silicides have larger formation enthalpies than germanides and stannides, (ii) Ir-containing materials have a larger stability area than Rh- and Co-containing materials, (iii) all nine carbides are thermodynamically unstable with respect to precipitation of graphite (minus signs in Figure 1a), and (iv) all nine unstable plumbides disproportionate into various combinations of binary metal alloys (Figure 1e). These theoretical results explain why no ternary plumbides or carbides have been previously reported in the V−IX−IV family of materials.

Regularities in the Predicted Equiatomic Crystal Structures. The two common structure types detected among stable materials of the V−IX−IV family are the MgSrSi-type, denoted here as S6 (space group *Pnma*, number 62) and the AgMgAs-type, denoted here as S1 (space group $F\bar{4}3m$, number 216). The S6 structure (Figure 2a) is related to

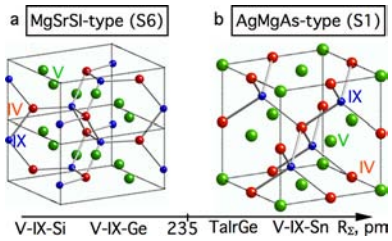

Figure 2. Two most common crystal structure types of equiatomic V−IX−IV materials: (a) MgSrSi-type structure S6; (b) AgMgAs-type filled tetrahedral structure S1. The common bottom axis delineates the structural preferences of V−IX−IV materials. In both parts of the figure, V is green, IX is blue, and IV is red.

the $PbCl_2$-type structure (S7) and Co_2Si-type structure (S40), and it has a four-fold coordinated IX−IV network filled with V atoms. The S1 is a filled tetrahedral structure (Figure 2b) that can be viewed as a IX−IV zincblende network filled with V atoms on interstitial sites or as a V−IV rocksalt network filled with IX atoms on interstitial sites. The structural preferences of V−IX−IV materials among S1 and S6 structure types can be delineated using the sum R_c of Shannon ionic radii[32] for V^{+III}, low-spin IX^{+III}, and IV^{+IV}. All 18 stable silicides and germanides with R_Σ less than 235 pm assume the S6 structure, and all 6 stable V−IX−IV stannides and TaIrGe with R_Σ more than 235 pm appear in the S1 crystal structure. This is a surprisingly simple delineation rule that would not be possible to comprehend without having a complete set of calculated thermodynamic stabilities (Figure 1) and predicted crystallographic structures (Figure 2 and Table S3, Supporting Information) of all V−IX−IV materials.

Predicted Structural Polymorphs for Equiatomic ABX. It is interesting to consider not only the ground-state structures but also the lowest energy metastable structures of the V−IX−IV materials. Metastable materials often have exciting and useful properties, such as transparent conductivity in the anatase polymorph of Nb doped TiO_2.[33] It is also well known that nonequilibrium synthesis routes, for example, physical vapor deposition techniques such as sputtering, can stabilize metastable compounds, for example, copper nitride.[34] Consequently, we report our predicted higher energy metastable structures (up to 150 meV/atom) for the eight missing and predicted stable V−IX−IV materials in Figure 3, along with the predicted ground-state structures. Interestingly, materials with the S1 ground-state structure have only a few likely polymorphs, whereas materials with the S6 ground-state structure have many excited configurations within this energy range. For example, S7, S14, and S40 structures have the same space group and the same Wyckoff position labels as S6 (Table S1, Supporting Information). Yet, in the example case of VIrSi, S14 and S7 are nearly degenerate with S6, but S40 is more than 150 meV/atom higher in energy (Figure 3). Therefore, we treat S6, S7, S14, and S40 as individual structure types despite their apparent similarity (Table S1, Supporting Information). Overall, these observations indicate that it may be easier to synthesize various polymorphs of the V−IX−IV materials with S6 structure than those with S1 structure.

Dynamic Phonon Stability. In addition to static thermodynamic stability of the theoretically predicted V−IX−IV materials, it is necessary to examine the phonons of the proposed new materials (Figure 1) in the predicted structures (Figure 2) to ensure that these materials are dynamically stable. We calculated phonon band structures of the four predicted stable V−IX−IV materials with S1 crystallographic structure using density functional perturbation theory (see Theoretical Methods). As shown in Figure S1 (Supporting Information), there are no negative phonon frequencies at all considered wave vectors; thus these four materials are dynamically stable. In the prototypical case of TaCoSn, the phonon calculation results are

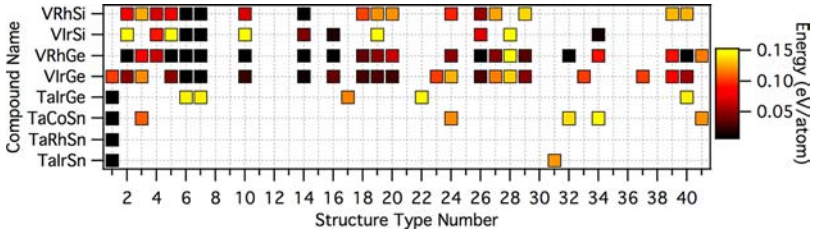

Figure 3. Calculated low-energy (0.00−0.15 eV/atom) crystal structures of eight missing but predicted stable equiatomic V−IX−IV materials. The names of the structure type numbers are listed in Table S1 (Supporting Information).

dx.doi.org/10.1021/ja311599g | J. Am. Chem. Soc. 2013, 135, 10048−10054

consistent with the results of GSGO calculations, because any material obtained as the statically stable structure in the GSGO method is guaranteed to be dynamically stable at the Γ point of its supercell. This in turn implies dynamic stability at other points of the K space that fold into the Γ point of the supercell.

EXPERIMENTAL REALIZATION OF PREDICTED NEW MATERIALS

Bulk Synthesis of TaCoS. To examine the theoretical predictions of new V−IX−IV compounds, we selected for experimental synthesis one member of this family of materials, TaCoSn. Bulk TaCoSn samples were synthesized from Ta and Co nanopowders, and micrometer-sized Sn powder in evacuated fused quartz ampules at 600 °C for 10 days (see the Experimental Methods). The experimental TaCoSn crystal structure was found to be consistent with the theoretical prediction (S1 structure), and the lattice parameter was 5.94 Å compared with 5.97 Å from theory (Table S4, Supporting Information). In addition to the TaCoSn phase, the products of the reaction contained Co-rich impurities, including Co_2Ta, CoSn, and $CoSn_2$, possibly due to presence of amorphous native oxide on the surfaces of Ta nanopowder precursor, which could have had kinetically limited the reaction process. Further regrinding and annealing for additional 10 days at the same temperature did not change the phase assemblage of the bulk TaCoSn sample.

Thin-Film Synthesis of TaCoSn. To improve purity, reactivity, and intermixing of the precursors, we deposited Ta−Co−Sn films (800 nm thickness) using combinatorial radio frequency cosputtering from Ta, Co, and Sn targets pointed at 45° toward stationary glass substrates heated to 550 °C in Ar atmosphere (see Experimental Methods). The combinatorial character of these experiments resulted in the specimens with a spread of stoichiometries around the Ta:Co:Sn = 1:1:1 composition (Figure 4a). As shown in Figure 4b, positions

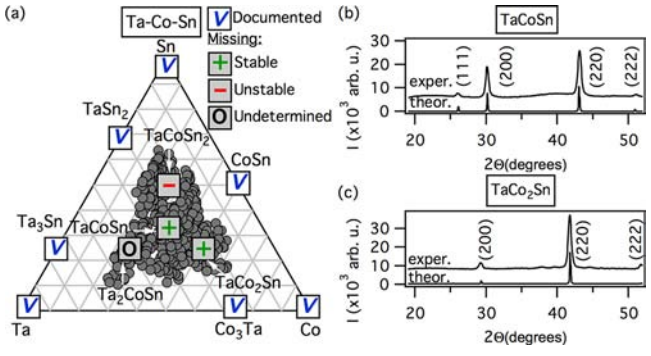

Figure 4. Experimental realizations of TaCoSn and $TaCo_2Sn$: (a) ternary Ta−Co−Sn composition space with two new ternary compounds and those documented binary and elemental materials that limit the stability of the ternary phases according to X-GSGO results. Experimental and theoretical XRD patterns of (b) TaCoSn and (c) $TaCo_2Sn$ thin films.

and intensities of the experimental TaCoSn X-ray diffraction (XRD) peaks agree well with the theoretical prediction (group IX atom in 4c position, Figure 2b and Table S5, Supporting Information) and differ from those reported previously for other materials in this group (group IV or group V atoms in 4c position).[18]

Thin-Films Experiment with Nonequiatomic Compositions. Although our main interest lies in equiatomic (1:1:1) V−IX−IV compounds that can be semiconductors on the basis of their closed-shell configuration, we did study in passing also other possible compositions around 1:1:1 (Figure 4a). Increasing Co content in the Ta−Co−Sn sample to 45−50 atomic % at the fixed Ta/Sn ratio led to experimental synthesis of a new compound with an XRD pattern that is consistent with $TaCo_2Sn$ material (Figure 4c). The $TaCo_2Sn$ Heusler structure can be derived from the TaCoSn half-Heusler structure (Table S6, Supporting Information) by populating the interstitial sites coordinated by four Ta and four Sn atoms with Co atoms (Table S7, Supporting Information). Together, $TaCo_2Sn$ and TaCoSn are the first two ternary materials reported in the Ta−Co−Sn system: prior to this study, only elemental and binary phases were known (those shown in Figure 4a plus Co_2Sn, Co_3Sn_2, $CoSn_2$, $CoSn_3$, Co_2Ta, $CoTa_2$, Ta_2Sn_3, and Ta_2Sn that do not limit the stability range of TaCoSn).

We note that, so far, we have not been able to experimentally identify false-negative results[35] of the theoretical predictions of missing materials, namely, experimentally stable compound predicted theoretically to be unstable. The absence of false-negatives is supported by unsuccessful synthesis attempts of missing and predicted unstable materials VCoSn (Figure 1) and $TaCoSn_2$ (Figure 4a).

ELECTRONIC STRUCTURE AND PHYSICAL PROPERTIES

Band Gaps in V−IX−IV Materials. We calculated basic electronic structure properties of all stable V−IX−IV materials and found that the materials with S1 structure, like TaCoSn, should be semiconductors. According to GGA+U DFT calculation results, these materials have greater than 1 eV band gaps in their nonmagnetic ground-state structure (Table S3, Supporting Information). The fact that all of these materials are made of three metallic elements yet have a band gap contrasts with conventional compound semiconductors (GaAs, ZnO, $CuInSe_2$), which are usually made of both metallic and nonmetallic elements. In contrast to nonmagnetic semiconducting V−IX−IV materials with S1 structure, the V−IX−IV materials that have S6 structure have an antiferromagnetic ground state and are metals with rather low density of states near the Fermi level.

Electronic Structure of TaCoSn. In order to shed light on the origin of the band gap in V−IX−IV materials with S1 structure, we calculated the symmetry projected partial density of states of TaCoSn in the S1 filled tetrahedral structure (Figure 2b) using the HSE06+GW method. The results of these calculations for Co and Ta are shown in Figure 5a, and a

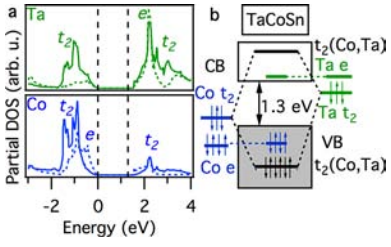

Figure 5. Band gap character in TaCoSn: (a) partial symmetry projected density of states for Ta and Co. (b) Resulting bonding scheme for Ta and Co derived from the density of states. In both parts of the figure, Ta is green, and Co is blue.

dx.doi.org/10.1021/ja311599g | J. Am. Chem. Soc. 2013, 135, 10048−10054

simplified energy level diagram describing the Co−Ta bonding scheme[36] is shown in Figure 5b. The d orbitals of Ta and Co split into t_2 and e symmetries in the crystal field created by the Sn ligands. The energy ordering of t_2 and e states is e below t_2 for Co (octahedral symmetry) and t_2 below e for Ta (tetrahedral symmetry).[37] Due to mutually tetrahedral coordination of Co and Ta atoms, (i) the Ta $t_2(d^3)$ interacts with the Co $t_2(d^3)$, creating a nonspin-polarized occupied t_2 (d^6) bonding state and an empty t_2 (d^0) antibonding state, and (ii) the occupied Co e (d^4) does not interact with the empty Ta e (d^0). Thus, the origin of the band gap in TaCoSn and other V−IX−IV materials is the combination of (i) splitting between the occupied bonding and empty antibonding states with t_2 symmetry, and (ii) the energy window between the pair of occupied and empty nonbonding states with e symmetry.

Charge Transfer in TaCoSn. It is interesting to note that, according to the theoretical calculations, TaCoSn features some degree of charge transfer from Ta to Co. The projection of the hybridized t_2 state onto the Co site has a larger intensity in the valence band, whereas the projection onto the Ta site has a larger intensity in the conduction band, as shown in Figure 5a, suggesting charge transfer from Ta to Co. This result is consistent with the energy ordering of the Ta 5d (−5.0 eV) and Co 3d (−8.8 eV) states in DFT calculations, that is likely to cause this charge transfer. The dynamic Born effective charges (Z^*), defined as the change of polarization created by atom displacement obtained from phonon calculations (Figure S1, Supporting Information), are Z^*(Ta) = +3.86, Z^*(Co) = −5.81, and Z^*(Sn) = +1.94 in TaCoSn, indicating the charge transfer from Ta to Co. The corresponding Born effective charges for other V−IX−IV compounds are given in Table S8 (Supporting Information), suggesting that the same phenomenon occurs in all of these materials. The relatively large amplitudes of Born effective charges Z^* above nominal charges are not uncommon and can be explained by p−d hybridizations effects.[38] Note that it has been previously reported that various charges calculated from first principles sometimes differ from traditional chemical point of view.[39]

Optical and Electrical Properties. TaCoSn is calculated to have an indirect band gap of 1.3 eV, according to HSE06+GW results. The absorption onset at 1.6 eV and high 10^5 cm^{-1} absorption coefficient above 1.8 eV (Figure 6a) suggests that TaCoSn may be suitable for thin-film photovoltaic absorber applications. Indeed, the calculated spectroscopic limited maximum efficiency (SLME)[40,41] reaches 20% value for the TaCoSn thin films with a thickness of only 0.4 μm. We attempted to verify experimentally these theoretical predictions and found significant subgap absorption in optical spectra of TaCoSn thin films. We attribute this absorption to high concentration of donorlike defects states that can merge into a defect band, since the TaCoSn samples had a low negative Seebeck coefficient (∼−5 μV/K) and a high electrical conductivity (∼1000 S/cm).

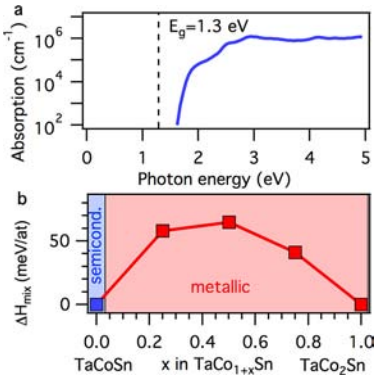

Figure 6. Calculated optical and alloy properties of TaCoSn: (a) optical absorption spectrum without excitonic effects; (b) mixing enthalpy as a function of TaCoSn−$TaCo_2Sn$ alloy composition.

Alloy and Defect Properties. To study the origin of the optical and electrical properties of TaCoSn thin films, we evaluated the mixing enthalpy of semiconducting TaCoSn and metallic $TaCo_2Sn$ alloy as a function of composition in the special quasirandom structure (SQS)[42] derived from the S1 filled tetrahedral structure. We found that the mixing enthalpy is 64 meV/atom for a 50%/50% alloy, and it gradually decreases toward the two end-point compounds (Figure 6b). This mixing enthalpy is smaller than the thermal energy of the substrate during thin-film synthesis (71 meV at 550 °C), and it is comparable to that of GaN−InN alloys,[43] which are not difficult to synthesize. Thus, it is likely that the experimentally observed subgap absorption and high electron density of the TaCoSn thin films is caused by disorder, specifically filling of some of the 50% unoccupied interstitial sites in the TaCoSn structure (Figure 2a) with Co atoms. To achieve semiconducting behavior of TaCoSn samples, the concentration of interstitial defect properties will have to be minimized, as has been previously demonstrated in related TiCoSb materials.[44] Further, to realize the full potential of TaCoSn as a first thin-film solar cell absorber made of all metallic elements, doping and interfaces of this material and its long-term stability under operating conditions will also have to be studied.

■ CONCLUSIONS

Theoretical prediction of eight new stable V−IX−IV materials and experimental realization of TaCoSn illustrate accelerated identification of missing stable materials using the inverse design approach. This study also enables identification of unexpected simple chemical trends in thermodynamic stability and crystallographic structures of V−IX−IV materials. Identification of several semiconductors among V−IX−IV materials made of all metallic elements exemplifies the benefits that come from broad screening of unconventional materials for useful properties. Another new material $TaCo_2Sn$ along with TaCoSn constitute the first two reported materials in the Ta−Co−Sn ternary materials system. Overall, we believe that our approach to missing materials that includes both theory and experiments can be widely applied to tackle the grand challenge of designing materials with tailored properties[45] in various fields of science and technology.

■ METHODS

Theoretical Methods. *First-Principles Total Energy Calculations.* Formation enthalpies (ΔH_f) were calculated using the projector-augmented wave (PAW) pseudopotential total energy method[46] with the exchange-correlation of Perdew−Burke−Ernzerhof (PBE)[47] as implemented in the Vienna ab initio simulation package (VASP).[48] We used an energy cutoff of 220−520 eV and reciprocal space grids with densities of $2\pi \times 0.068$ Å^{-1} and $2\pi \times 0.051$ Å^{-1} for relaxation and static calculations, respectively. For transition metals, we used the DFT +U method[49] with reported previously U values.[28] We investigated ferromagnetic, antiferromagnetic, and random spin configurations of the unit cell, initializing both high- and low-spin values on the transition metals. To correct systematic DFT errors in compound formation enthalpies, we use the method, where a set of 252 measured

dx.doi.org/10.1021/ja311599g | J. Am. Chem. Soc. 2013, 135, 10048−10054

enthalpies of formation ΔH_f values for binary compounds (pnictides, chalcogenides, and halides) was used to fit to "fitted elemental-phase reference energies" (FERE) for 50 elements.[28,29] This resulted in calculations of the enthalpies of formation to with a root-mean-square error of 0.07 eV/atom.

Structure Prototyping (Step 1a). We construct a set of crystal structure types for a given stoichiometry, compute the total energy of each missing material in each of the structure prototypes subject to local relaxations (see Table S1, Supporting Information as an example for 1:1:1 materials), and then, select from this list the lowest-energy structure (see Table S2, Supporting Information as an example for the $TaCo_2Sn$ 1:2:1 material). The list of candidate structure types (Table S1, Supporting Information) is created from those that are known from existing ABX compounds in the ICSD and other databases.

Genetic Algorithm Calculations (Step 1b). The initial GSGO structure search was performed for structures with up to six atoms (see below). The population size was set to 64, and the 16 worst individuals were replaced by offspring at each generation. The rate of crossover versus mutation was set to 0.7. Two independent GSGO runs with up to 12 generations were performed for each run.

For the composition-dependent X-GSGO method,[31] we evaluated the ΔH_f as a function of composition, searching for the composition and its lowest-energy crystal structure that do not disproportionate into nearby compositions and structures (convex hull). The binary compounds on the convex hull function were taken from the ICSD.[18] The X-GSGO search was performed for structures with less than eight atoms, superseding the GSGO calculations with six atoms described above. Three independent X-GSGO runs with 15 or more generations were performed per run. The population size and the rate of crossover versus mutation are the same as in the GSGO search.

Calculations of Phonon Dispersion (Step 1c). To calculate phonon dispersion and Born effective charges,[50] we used density functional perturbation theory as implemented in Quantum-Espresso.[51] Norm-conserving GGA pseudopotentials and a plane-wave cutoff of 100 Ry were adopted. The crystal structures of all considered materials have been fully relaxed by GGA without Hubbard U by Quantum-Espresso before phonon calculations (Figure S1, Supporting Information).

Calculations of Thermodynamic Stability with Respect to Reported Competing Phases (Step 2). Thermodynamic stability of the ABX compounds was determined from the calculated ΔH_f of each ABX phase and its competing phases by simultaneously solving a set of inequalities in a three-dimensional space of chemical potentials $\Delta\mu_A$, $\Delta\mu_B$, and $\Delta\mu_X$.[16,17] For all competing elemental phases, we used inequalities of the form $\Delta\mu_A < 0$. For all competing binary phases, A_aB_b, we used inequalities of the form $a\Delta\mu_A + b\Delta\mu_B < \Delta H_f$ (A_aB_b). For all competing ternary phases $A_aB_bX_x$, we used inequalities of the form $a\Delta\mu_A + b\Delta\mu_B + x\Delta\mu_X < \Delta H_f$ ($A_aB_bX_x$). This three-dimensitonal space of chemical potentials was reduced to two dimensions by the $\Delta\mu_A + \Delta\mu_B + \Delta\mu_X = \Delta H_f$ (ABX) equation (Figure S2, Supporting Information). The values of $\Delta\mu_A$ and $\Delta\mu_B$ where all inequalities are satisfied define the stability area of the ABX compound. Both reported (step 2a) and unreported (step 2b) competing phases are taken into account for this analysis.

Electronic Structure Calculations. Electronic structure (band gap, partial density of states, and absorption coefficient) was calculated by applying partially self-consistent GW_0 approximation[52] on top of hybrid functional (HSE06) wave functions.[53] Results of these electronic structure calculations were used to calculate SLME,[40,41] which explicitly takes into account the band gap, the shape of absorption spectra, and the material-dependent nonradiative recombination losses.

Alloy Calculations. We evaluated the mixing enthalpy of the TaCoSn−$TaCo_2Sn$ alloy as a function of composition using the special quasi-random structures (SQS)[42] that minimize the differences of correlation functions of the supercell structures and the ideal random structure.[54] The supercell structures contain 64 atomic sites; 48 of the sites are occupied by Ta, Co, and Sn, forming the FTS structure; the remaining 16 sites are occupied by either Co atoms or vacancies. The 50%/50% SQS structure has its first to seventh pair correlation functions equal to the ideal random case. The 25%/75% (75%/25%) SQS structure has its first to third pair correlation functions equal to the ideal random case, and its absolute value of fourth pair correlation function is 0.04 smaller than the ideal random value 0.25.

Experimental Methods. *Bulk Synthesis.* The powder metallurgy method was used for bulk synthesis of TaCoSn. Powders of tantalum (60−80 nm, 99.9% purity), cobalt (25−30 nm, 99.8% purity), and tin (150 μm, 99.5% purity) were used as precursors. The powders were weighed with 0.1 mg accuracy and mixed thoroughly by hand. A pellet 7.94 mm in diameter was cold-pressed at ∼120 MPa and sealed in an evacuated fused quartz ampule with a residual pressure of ∼0.1 mTorr. The sample was then annealed for 10 days at 600 °C.

Bulk Characterization. XRD measurements were performed using a Scintag XDS2000 diffractometer equipped with a Cu Kα radiation source and a liquid nitrogen cooled Ge detector. The lattice constant was determined using an internal Si standard, a step size of 0.02°, a dwell time of 1 s, and "whole pattern fitting" Rietveld refinement in the JADE 9 software package. Impurity phases were also identified using JADE 9.

Thin-Film Growth. TaCoSn thin films of 320 nm thickness were deposited using combinatorial radio frequency cosputtering from Ø50 mm Ta, Co, and Sn targets (99.9% purity) pointed at a 45° angle with respect to the substrate. Stationary glass substrates were heated to 550 °C in 2×10^{-5} atm of Ar atmosphere (99.999% pure) in a vacuum chamber with 10^{-9} atm base pressure. VCoSn thin-film synthesis was performed in a similar way, but a V target was used instead of a Ta target. More details of the combinatorial synthesis apparatus have been previously described.[55]

Thin-Film Characterization. The crystal structure of TaCoSn thin films was measured using XRD in Cu Kα radiation. The resulting XRD patterns were subjected to subtraction of a separately measured XRD background that results from the glass substrate. Composition and thickness of the thin films was determined from X-ray fluorescence measurements. More details of the characterization instruments have been previously reported.[56]

■ ASSOCIATED CONTENT

Ⓢ Supporting Information

Phonon dispersion curves of four V−IX−IV materials; structure types of ABX compounds; 10 lowest energy crystal structures for $TaCo_2Sn$; calculated properties of stable V−IX−IV materials; thermodynamic stability analysis, crystallographic information, and atomic coordinates for TaCoSn and $TaCo_2Sn$. This material is available free of charge via the Internet at http://pubs.acs.org.

■ AUTHOR INFORMATION

Corresponding Author

alex.zunger@gmail.com

Notes

The authors declare no competing financial interest.

■ ACKNOWLEDGMENTS

This work is supported by the U.S. Department of Energy, Office of Science, Basic Energy Sciences, under contract no. DE-AC36-08GO28308 to NREL as a part of the DOE Energy Frontier Research Center "Center for Inverse Design". TaCoSn bulk XRD patterns were collected and refined at the J. B. Cohen X-ray Diffraction Facility supported by the MRSEC program of the National Science Foundation (DMR-1121262) at the Materials Research Center of Northwestern University. We are grateful to V. Stevanovic for important discussions. X.Z. also acknowledges the administrative support of REMRSEC under NSF grant number DMR-0820518, Colorado School of Mines, Golden, Colorado.

REFERENCES

(1) Curtarolo, S.; Hart, G. L. W.; Nardelli, M. B.; Mingo, N.; Sanvito, S.; Levy, O. *Nat. Mater.* **2013**, *12*, 191−201.
(2) Meredig, B.; Wolverton, C. *Nat. Mater.* **2013**, *12*, 123−127.
(3) Wood, D. M.; Zunger, A.; de Groot, R. *Phys. Rev. B* **1985**, *31*, 2570−2573.
(4) Carlsson, A. E.; Zunger, A.; Wood, D. M. *Phys. Rev. B* **1985**, *32*, 1386−1389.
(5) Nowotny, H.; Sibert, W. Z. *Z. Metallkd.* **1941**, *33*, 391.
(6) Juza, R.; Hund, F. *Naturwissenschaften* **1946**, *33*, 121.
(7) Heusler, F. *Verh. Dtsch. Phys. Ges.* **1903**, *5*, 219.
(8) de Groot, R. A.; Mueller, F. M.; van Engen, P. G.; Buschow, K. H. J. *Phys. Rev. Lett.* **1983**, *50*, 2024−2027.
(9) Yang, J.; Li, H.; Wu, T.; Zhang, W.; Chen, L.; Yang, J. *Adv. Funct. Mater.* **2008**, *18*, 2880−2888.
(10) Kieven, D.; Klenk, R.; Naghavi, S.; Felser, C.; Gruhn, T. *Phys. Rev. B* **2010**, *81*, 075208.
(11) Roy, A.; Bennett, J. W.; Rabe, K. M.; Vanderbilt, D. *Phys. Rev. Lett.* **2012**, *109*, 037602.
(12) Bennett, J. W.; Garrity, K. F.; Rabe, K. M.; Vanderbilt, D.. *Phys. Rev. Lett.* **2012**, *109*, 167602.
(13) Bennett, J. W.; Garrity, K. F.; Rabe, K. M.; Vanderbilt, D. *arXiv:1210.7116 [cond-mat.mtrl-sci]* **2012**, 5.
(14) Chadov, S.; Qi, X.; Kübler, J.; Fecher, G. H.; Felser, C.; Zhang, S. C. *Nat. Mater.* **2010**, *9*, 541−545.
(15) Lin, H.; Wray, L. A.; Xia, Y.; Xu, S.; Jia, S.; Cava, R. J.; Bansil, A.; Hasan, M. Z. *Nat. Mater.* **2010**, *9*, 546−549.
(16) Zhang, X.; Yu, L.; Zakutayev, A.; Zunger, A. *Adv. Funct. Mater.* **2012**, *22*, 1425−1435.
(17) Zhang, X.; Stevanović, V.; d'Avezac, M.; Lany, S.; Zunger, A. *Phys. Rev. B* **2012**, *86*, 014109.
(18) Bergerhoff, G.; Brown, I. D. In *Crystallographic Databases*; Allen, F. H., Bergerhoff, G., Sievers, R., Eds.; International Union of Crystallography: Chester, U.K., 1987.
(19) ICDD PDF: International Centre For Diffraction Data, Powder Diffraction File (Newtown Square, PA).
(20) Villars, P.; Calvert, L. D. *Pearson's Handbook of Crystallographic Data for Intermetallic Phases*; ASM International: Materials Park, OH, 1991.
(21) Berger, L. I. Semiconductor Materials. In *Physical Sciences References*; CRC Press: Boca Raton, FL, 1996.
(22) Zhang, S. B.; Wei, S.-H.; Zunger, A. *Phys. Rev. Lett.* **1997**, *78*, 4059−4062.
(23) Hautier, G.; Fischer, C. C.; Jain, A.; Mueller, T.; Ceder, G. *Chem. Mater.* **2010**, *22*, 3762−3767.
(24) Taylor, R. H.; Curtarolo, S.; Hart, G. L. W. *Phys. Rev. B* **2011**, *84*, 084101.
(25) Nørskov, J. K.; Bligaard, T.; Rossmeisl, J.; Christensen, C. H. *Nat. Chem.* **2009**, *1*, 37−46.
(26) Chen, H.; Hautier, G.; Ceder, G. *J. Am. Chem. Soc.* **2012**, *134*, 19619−19627.
(27) Hautier, G.; Jain, A.; Ong, S. P. *J. Mater. Sci.* **2012**, *47*, 7317−7340.
(28) Lany, S. *Phys. Rev. B* **2008**, *78*, 245207.
(29) Stevanović, V.; Lany, S.; Zhang, X.; Zunger, A. *Phys. Rev. B* **2012**, *85*, 115104.
(30) Trimarchi, G.; Zunger, A. *Phys. Rev. B* **2007**, *75*, 104113.
(31) Trimarchi, G.; Freeman, A. J.; Zunger, A. *Phys. Rev. B* **2009**, *80*, 092101.
(32) Shannon, R. D.; Prewitt, C. T. *Acta Crystallogr., Sect. B* **1969**, *25*, 925−946.
(33) Furubayashi, Y.; Hitosugi, T.; Yamamoto, Y.; Inaba, K.; Kinoda, G.; Hirose, Y.; Shimada, T.; Hasegawa, T. *Appl. Phys. Lett.* **2005**, *86*, 252101.
(34) Juza, R.; Hahn, H. *Z. Anorg. Allg. Chem.* **1939**, *241*, 172.
(35) Vidal, J.; Zhang, X.; Yu, L.; Luo, J.-W.; Zunger, A. *Phys. Rev. B* **2011**, *84*, 041109(R).
(36) Öğüt, S.; Rabe, K. M. *Phys. Rev. B* **1995**, *51*, 10443−10453.
(37) Miessler, G. L.; Tarr, D. A. *Inorganic Chemistry*, 3rd ed.; Pearson Prentice Hall, Upper Saddle River, NJ, 2003.
(38) Ghosez, Ph.; Michenaud, J.-P.; Gonze, X. *Phys. Rev. B* **1998**, *58*, 6224.
(39) Raebiger, H.; Lany, S.; Zunger, A. *Nature* **2008**, *453*, 763−766.
(40) Yu, L.; Zunger, A. *Phys. Rev. Lett.* **2012**, *108*, 068701.
(41) Yu, L.; Kokenyesi, R. S.; Keszler, D. A.; Zunger, A. *Adv. Energy Mater.* **2013**, *3*, 43−48.
(42) Wei, S.-H.; Ferreira, L. G.; Bernard, J. E.; Zunger, A. *Phys. Rev. B* **1990**, *42*, 9622−9649.
(43) Liu, J. Z.; Zunger, A. *Phys. Rev. B* **2008**, *77*, 205201.
(44) Ouardi, S.; Fecher, G. H.; Felser, C.; Schwall, M.; Naghavi, S. S.; Gloskovskii, A.; Balke, B.; Hamrle, J.; Postava, K.; Pistora, J.; Ueda, S.; Kobayashi, K. *Phys. Rev. B* **2012**, *86*, 045116.
(45) Fleming, G. R.; Ratner, M. A. *Phys. Today* **2008**, *61*, 28−33.
(46) Zunger, A.; Perdew, J. P.; Oliver, G. L. *Solid State Commun.* **1980**, *34*, 933−936.
(47) Perdew, J. P.; Burke, K.; Ernzerhof, M. *Phys. Rev. Lett.* **1996**, *77*, 3865.
(48) Kresse, G.; Furthmüller, J. *Comput. Mater. Sci.* **1996**, *6*, 15−50.
(49) Dudarev, S. L.; Botton, G. A.; Savrasov, S. Y.; Humphreys, C. J.; Sutton, A. P. *Phys. Rev. B* **1998**, *57*, 1505−1509.
(50) Baroni, S.; de Gironcoli, S.; Dal Corso, A.; Giannozzi, P. *Rev. Mod. Phys.* **2001**, *73*, 515−562.
(51) Giannozzi, P.; Baroni, S.; Bonini, N.; Calandra, M.; Car, R.; Cavazzoni, C.; Ceresoli, D.; Chiarotti, G. L.; Cococcioni, M.; Dabo, I.; et al. *J. Phys.: Condens. Matter* **2009**, *21*, 395502.
(52) Shishkin, M.; Kresse, G. *Phys. Rev. B* **2007**, *75*, 235102.
(53) Heyd, J.; Scuseria, G. E.; Ernzerhof, M. *J. Chem. Phys.* **2003**, *118*, 8207.
(54) van de Walle, A.; Asta, M.; Ceder, G. *Calphad* **2002**, *26*, 539−553.
(55) Zakutayev, A.; Perkins, J. D.; Parilla, P. A.; Widjonarko, N. E.; Sigdel, A. K.; Berry, J. J.; Ginley, D. S. *MRS Commun.* **2011**, *1*, 23−26.
(56) Zakutayev, A.; Paudel, T. R.; Ndione, P. F.; Perkins, J. D.; Lany, S.; Zunger, A.; Ginley, D. S. *Phys. Rev. B* **2012**, *85*, 085204.